Journal of Materials Chemistry C

Accepted Manuscript

This article can be cited before page numbers have been issued, to do this please use: Y. He, J. Quinn, D. Hou, J. H.L. Ngai and Y. Li, *J. Mater. Chem. C*, 2017, DOI: 10.1039/C7TC03584E.

ROYAL SOCIETY OF CHEMISTRY

rsc.li/materials-c

View Article Online
DOI: 10.1039/C7TC03584E

Journal Name

ARTICLE

A small bandgap (3*E*,7*E*)-3,7-bis(2-oxoindolin-3-ylidene)benzo[1,2-*b*:4,5-*b'*]difuran-2,6(3*H*,7*H*)-dione (IBDF) based polymer semiconductor for near-infrared organic phototransistors

Received 00th January 20xx,
Accepted 00th January 20xx

DOI: 10.1039/x0xx00000x

www.rsc.org/

Yinghui He,[a‡] Jesse T. E. Quinn,[a‡] Dongliang Hou [a,b‡], Jenner H.L. Ngai[a] and Yuning Li[a]

A (3*E*,7*E*)-3,7-bis(2-oxoindolin-3-ylidene)benzo[1,2-*b*:4,5-*b'*]difuran-2,6(3*H*,7*H*)-dione (IBDF)-based small bandgap donor-acceptor (D-A) polymer (**PIBDFBTO-HH**) was synthesized, which contains a strategically chosen solubilizing electron-rich building block, 3,3'-bis(dodecyloxy)-2,2'-bithiophene (BTO) as a donor. **PIBDFBTO-HH** has a very small band gap of 0.95 eV, absorbing up to 1700 nm in the near-infrared (NIR) region, which enables its application in NIR photodetection. This polymer exhibits efficient ambipolar charge transport properties with balanced hole and electron mobilities of up to 0.16 $cm^2 V^{-1} s^{-1}$ and 0.14 $cm^2 V^{-1} s^{-1}$, respectively, in organic thin film transistors (OTFTs) in the absence of light. In the p-channel operation regime, the organic phototransistor (OPT) devices based on **PIBDFBTO-HH** demonstrated photosensitivities (P) of 130 and 40 under the illumination of 850 nm and 940 nm LED light sources, respectively. The photoresponsivity (R) under the 940 nm LED reached 450 mA W^{-1}. On the contrary, in the n-channel operation regime, a negative photoresponse, namely a decrease in the drain current, was observed, which is accounted for the increased number of trapped electrons that offset the applied gate bias.

Introduction

π-Conjugated polymers have been extensively studied as channel semiconductors in organic thin film transistors (OTFTs) due to their excellent solution processability, large-area coverage, mechanical robustness, and low cost.[1–5] Donor–acceptor (D–A) polymers, a special class of π-conjugated polymers that are comprised of D-A arrangements in the backbone, have demonstrated very high charge carrier mobilities in OTFTs.[6–9] One key reason for their high charge transport performance is that the strong interchain D–A interaction will induce ordered chain packing and shorten the π–π stacking distance, facilitating the interchain charge transport.[10,11]

An organic phototransistor (OPT) is an OTFT device with its channel organic semiconductor being able to detect and convert optical inputs into electrical signals.[12,13] Compared to organic photodiodes (OPDs), OPTs allow for facile integration into electro-optical logic circuits[14] and unlike OPDs, OPTs have two operational mechanisms, controlled by tuning gate voltage, enabling greater sensitivity and lowered noise.[15] Polymer-based OPTs have numerous advantages such as advantages of low cost, lightweight, and flexibility compared to their counterparts such as small molecules, inorganic materials and quantum dots (QDs) based phototransistors.[16–19] The bulk of OPT research has been carried out on the UV and visible light detection, while near-infrared (NIR) OPTs were less explored due to the lack of suitable polymer semiconductors that can both detect NIR signals and possess good field-effect transistor performance.[20–22] Recently, NIR OPTs have gained intensified attention due to their promising applications in optoelectronics including security, military, and medical diagnosis equipment.[23,24] Most of the NIR OPTs used polymer blends, emulating the bulk heterojunction structures commonly used in solar cell studies, to realize NIR absorption.[17,23,25] For example, Sun *et al.* reported a hybrid PbS QD and poly(3-hexylthiophene) OPT, which showed a photoresponsivity of up to 2×10^4 A W^{-1} using an 895 nm centered LED.[23] However, the polymer blends may suffer from a long-term phase stability issue,[25] which is frequently observed for other organic electronic devices.[26,27] For the single component OPTs, Li *et al.* developed a NIR OPT using the n-type small molecule 4,4-difluoro-4-bora-3a,4a-diaza-s-indacene (BODIPY-BF2), which absorbs in the NIR region (up to 1000 nm).[28] A photoresponsivity of up to 7.82×10^3 A W^{-1} was realized with a 940 nm LED. D-A polymers usually have small band gaps because of the intramolecular charge transfer (ICT) from the donor unit to the acceptor unit.[29–32] Müllen *et al.* recently reported a phenanthrene condensed thiadiazoloquinoxaline D–A polymer, which has a small optical bandgap of 0.80 eV with a broad absorption in 700–1500 nm

[a] *Department of Chemical Engineering and Waterloo Institute for Nanotechnology (WIN), University of Waterloo, 200 University Ave West, Waterloo, Ontario, N2L 3G1, Canada. *E-mail: yuning.li@uwaterloo.ca; Fax: +1 519-888-4347; Tel: +1 519-888-4567 ext. 31105*
[b] *Department of Computer Application Engineering, College of Engineering, Shanghai Polytechnic University, Shanghai, 201209, P.R. China*
†Electronic Supplementary Information (ESI) available. See DOI: 10.1039/x0xx00000x
‡ These authors made equal contributions.

View Article Online
DOI: 10.1039/C7TC03584E

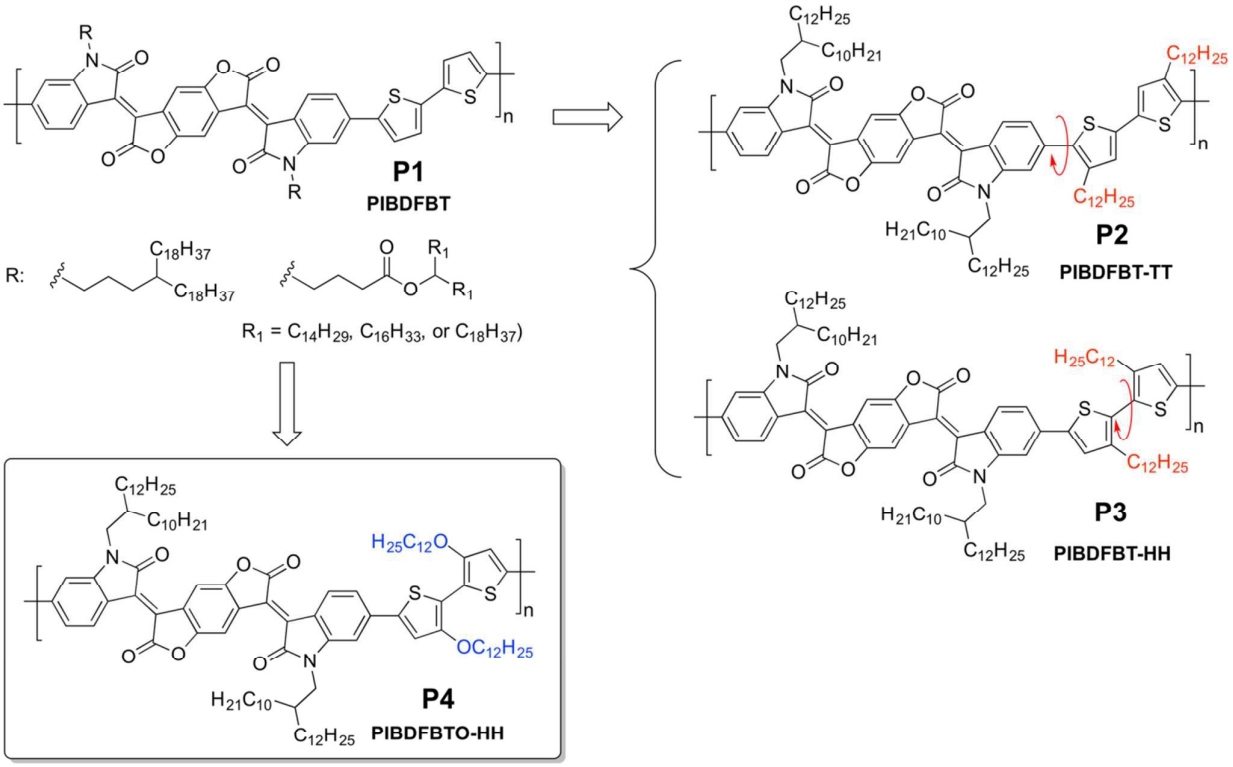

Figure 1. The chemical structures of **IBDFBT** copolymers.

region).[33] This polymer showed ambipolar charge transport performance with balanced hole and electron mobilities of up to 0.09 $cm^2 V^{-1} s^{-1}$ and 0.06 $cm^2 V^{-1} s^{-1}$ in OTFTs. OPTs with this polymer exhibited very high photoresponsivity of up to 400 A W^{-1} under white light in the p-channel operation regime; however, a rather low photosensitivity of 0.5 was obtained.

Recently our group developed a strong electron acceptor building block, (3*E*,7*E*)-3,7-bis(2-oxoindolin-3-ylidene)benzo[1,2-*b*:4,5-*b'*]difuran-2,6(3*H*,7*H*)-dione (IBDF), which has been used for the construction of some of the best performing unipolar n-type and ambipolar polymer semiconductors for OTFTs.[9,34–43] The D-A copolymers of IBDF and non-substituted bithiophene (BT), PIBDFBT (Figure 1), showed quite small band gaps (~1.3 eV) with the longest absorption wavelength extending to ~1000 nm.[39] By substitution of the bithiophene unit with alkyl (dodecyl) chains, Wang *et al.* slightly reduced the band gap of the resulting two polymers, **PIBDFBT-HH** (with head-to-head substitution on BT) and **PIBDFBT-TT** (with tail-to-tail substitution on BT) (Figure 1), to 1.24 eV and 1.26 eV, respectively. **PBIBDFBT-TT** exhibited ambipolar charge transport with hole and electron mobilities of up to 0.02 $cm^2 V^{-1} s^{-1}$ and 0.04 $cm^2 V^{-1} s^{-1}$, respectively, in OTFTs.[44] Single-component NIR OPTs of this polymer achieved photoresponsivity of up to 47.1 A W^{-1}. However, the absorption profile of **PBIBDF-TT** only reached 998 nm with a λ_{max} at ~800 nm,[43] which may not be optimal for certain NIR detection applications.[45]

Herein, we present a new IBDFBT copolymer, **PIBDFBTO-HH** (Figure 1), which has a head-to-head alkoxy substituted bithiophene (BTO) unit as the donor, aiming to achieve NIR detection in longer wavelength regions. The stronger electron donating and sterically less demanding alkoxy substituents on the bithiophene in **PIBDFBTO-HH** than the alkyl substituents in **PIBDFBT-HH** could enhance the intramolecular charge transfer (ICT) and render the polymer backbone much more coplanar, resulting in a very small bandgap of 0.95 eV with a broad absorption range in NIR region up to ~1700 nm. In addition, this polymer showed balanced ambipolar charge transport characteristics with hole mobility of up to 0.16 $cm^2 V^{-1} s^{-1}$ and electron mobility of up to 0.14 $cm^2 V^{-1} s^{-1}$ in bottom-gate bottom-contact (BGBC) devices. In OPTs, **PIBDFBTO-HH** exhibited photoresponsivity of up to 0.45 A W^{-1} with very short rise time of 9.4 ms and fall time of 6.6 ms under illumination by a 940 nm LED light source. A photosensitivity of up to 130 was achieved. Our results showed that **PIBDFBTO-HH** is a promising material for long wavelength NIR photodetectors.

Results and Discussion

View Article Online
DOI: 10.1039/C7TC03584E
Journal Name ARTICLE

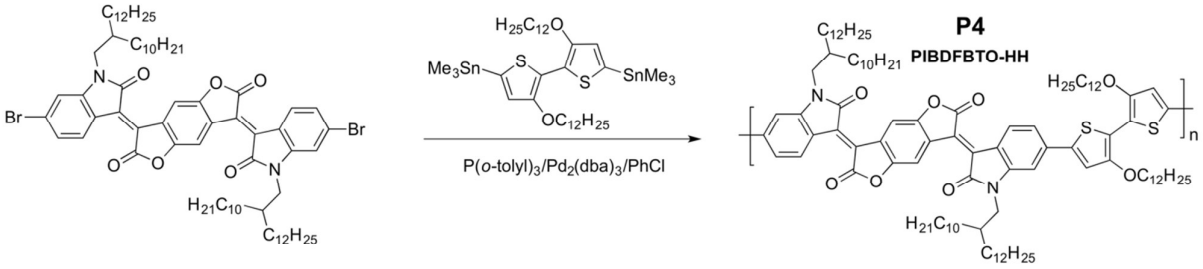

Scheme 1. Synthetic route to **P4**.

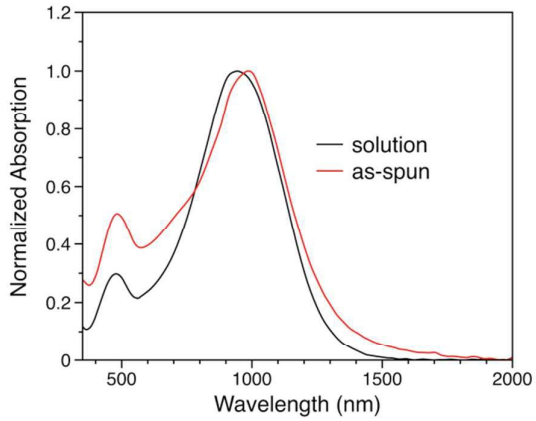

Figure 2. The UV-VIS-NIR absorption profile of **P4**.

For the convenience of discussion, polymers **PIBDFBT**, **PINDFBT-TT**, **PIBDFBT-HH** and **PIBDFBTO-HH** are denoted as **P1**, **P2**, **P3**, and **P4**, respectively (Figure 1). Our study began with conducting a theoretical comparison of the optimized geometries and frontier energy levels of **P4** to those of two previously reported IBDFBT polymers, **P1**,[9] which has unsubstituted bithiophene units, and **P3**,[43] which has head-to-head dodecyl substituents on the bithiophene units. DFT calculations of the molecular geometries and electronic structures were performed for their isolated (gas phase) methyl-substituted dimers **P1-Me, P3-Me** and **P4-Me** (Figure S1 and S2 in the ESI), using the B3LYP functional and the 6–31G(d) basis set as implemented in Gaussian 09.[46] As shown in Figure S1, **P4-Me** showed the smallest bandgap of 1.43 eV, compared to **P1-Me** (1.80 eV) and **P3-Me** (1.88 eV). The significantly reduced bandgap of **P4-Me** mainly originates from the elevated HOMO energy level. While all three dimers have very similar LUMO energy levels between -3.4 and -3.5 eV, **P4-Me** has a much higher HOMO energy level of -4.82 eV than those of the other two (-5.34 eV for **P3-Me** and -5.30 eV for **P1-Me**). The results clearly indicate that a strong electron donating effect from the alkoxyl groups can effectively reduce the bandgap of the polymer by raising the HOMO energy level. From the optimized geometries, the dihedral angles between IBDF unit and bithiophene unit were found to be 19.2 °, 22.1 ° and 16.1 ° for **P1-Me, P3-Me** and **P4-Me**, respectively, indicating that **P4-Me** has a slightly more coplanar IBDF-thiophene linkage. As for the coplanarity between the two thiophene units, **P4-Me** shows an almost coplanar structure with a very small dihedral of 0.3 °, while the other two dimers are quite twisted with dihedral angles of 24.4 ° for **P1-Me** and 44.7 ° for **P3-Me**. With the oxygen atom inserted between the thiophene unit and the alkyl chain in **P4-Me**, the steric effect between the two methoxy-substituted thiophene units is minimized. The more planar backbone of **P4-Me** would allow more extended delocalization of π-electrons, which is another factor that contributes to the much smaller bandgap of **P4-Me** compared to the other two dimers (Figure S2).

P4 was synthesized by reacting 3,7-bis((*E*)-6-bromo-1-(2-decyltetradecyl)-2-oxoindolin-3-ylidene)-3,7-dihydrobenzo[1,2-*b*:4,5-*b*']difuran-2,6-dione[34] and (3,3'-bis(dodecyloxy)-[2,2'-bithiophene]-5,5'-diyl)bis(trimethylstannane)[47] *via* Stille coupling polymerization (Scheme 1). The crude polymer was subject to Soxhlet extraction with acetone, hexanes and chloroform. After drying the chloroform-extracted fraction, **P4** was obtained in a nearly quantitative yield (~98%). With the addition of alkoxy side chains on the thiophene units, **P4** shows good solubility (>10 mg mL^{-1}) in certain organic solvent such as chloroform. **P4** has a number average molecular weight (M_n) of 23.3 kDa and a polydispersity index (PDI) of 8.0 as determined by high temperature gel-permeation chromatography (HT-GPC) at 140 °C using polystyrene as standards. The thermal stability of **P4** was characterized using thermogravimetric analysis (TGA). The 5% weight loss was found at 337 °C under nitrogen (Figure S3), indicating a good thermal stability of this polymer. We also conducted differential scanning calorimetry (DSC) measurement on **P4** (Figure S4). However, no noticeable endo- or exothermic transitions were observed in the range between -20 °C and 300 °C, indicating the rather poor crystallinity of this polymer, which was further verified by the XRD results (to be discussed later).

The UV-Vis-NIR absorption spectra of **P4** in dilute solution and thin film (Figure 2) showed a broad absorption in the NIR region of spectrum (with noticeable absorption even at ~1700 nm) as a result of the efficient intramolecular charge transfer (ICT) between IBDF and BTO moieties. The maximum absorption wavelength (λ_{max}) was red-shifted to 986 nm in thin film from 944 nm in solution. This red-shift can be explained by the chain packing in the solid state that makes the backbone more coplanar and induces interchain electronic interactions, leading to a reduced bandgap. Using the absorption onset (~1300 nm) of the thin film spectrum, a very small bandgap of 0.95 eV was calculated. In contrast, the bandgaps of **P1** (1.31 eV) and **P3** (1.24 eV),[9,37] based on the onset of absorption of their films, are much larger than that of **P4**. The above results

View Article Online
DOI: 10.1039/C7TC03584E

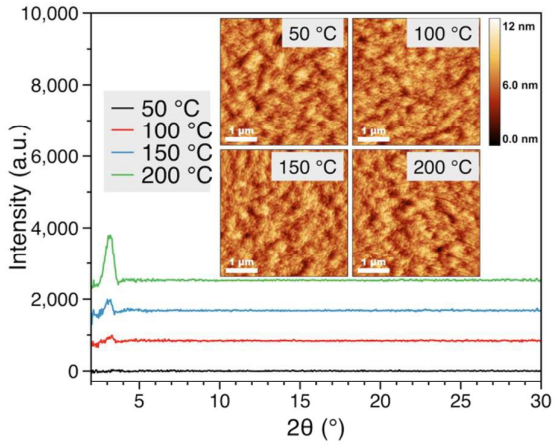

Figure 3. XRD of **P4** at different annealing temperatures. Inset: AFM height images (4 μm × 4 μm) at corresponding annealing temperatures.

correlate with the trend observed with the DFT simulations on their respective dimers and supports our strategy of using BTO as a donor building block to successfully shift the absorption profile further into the NIR region.

The electrochemical properties of **P4** thin films were measured by cyclic voltammetry (CV) (Figures S5 and S6) in a 0.1 M tetrabutylammonium hexafluorophosphate solution in anhydrous acetonitrile at a scan rate of 50 mV s^{-1}. The onset oxidation potential of **P4** was 0.56 V, which was used to calculate the HOMO energy of this polymer to be -5.33 eV using ferrocene as a standard. Similarly, the LUMO energy was calculated to be -3.86 eV from the onset reduction potential (-0.91 V). A band gap of 1.47 eV was thus obtained with this electrochemical measurement. The relatively low LUMO energy (close to -4.0 eV[48] that is the minimum value required for stable electron transport) and relatively high HOMO of **P4** make it potentially a suitable material for ambipolar charge transport.

The crystallinity of the polymer thin films annealed at different temperatures was studied by reflective XRD. As shown in Figure 3, the film annealed at 50 °C showed very weak diffraction peaks, corresponding to an almost amorphous thin film. With 100 °C annealing, the diffraction peak (100) representing the interlamellar distance appeared and became more prominent for the film annealed at higher temperatures (150 and 200 °C), indicating more ordered chain

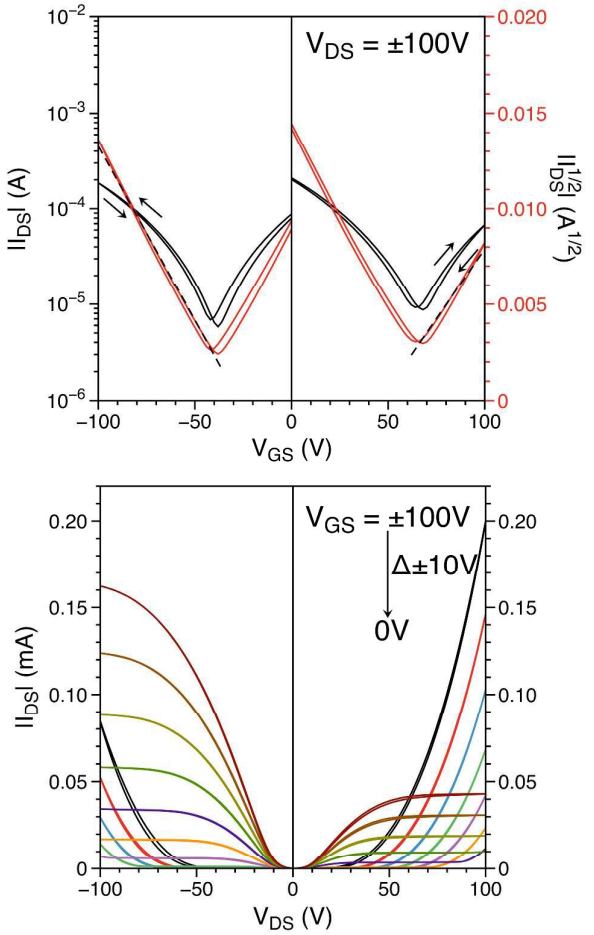

Figure 4. Transfer (top) and output (bottom) curves (with forward and reverse sweeps) of an OTFT with 150 °C -annealed **P4**.

packing in the films. The *d*-spacing for the lamellar distance was determined to be 2.76 nm. The AFM height images of the resulting annealed thin films (inset of Figure 3) show little change in the surface morphology for films annealed at different temperatures. All the films are quite smooth with root-mean-square roughness of ~1 nm.

To investigate the charge transport properties of **P4**, bottom-gate bottom-contact (BGBC) OTFTs were fabricated by spin-coating a solution of this polymer in chloroform onto dodecyltrichlorosilane (DDTS) treated Si/SiO_2 wafer substrates

Annealing temperature (°C)	Hole transport				Electron transport			
	Ave. μ ($cm^2 V^{-1} s^{-1}$)	Max. μ ($cm^2 V^{-1} s^{-1}$)	V_{th} (V)	$I_{on/off}$	Ave. μ ($cm^2 V^{-1} s^{-1}$)	Max. μ ($cm^2 V^{-1} s^{-1}$)	V_{th} (V)	$I_{on/off}$
50	0.14±0.02	0.15	-0.6	~100	0.10±0.01	0.12	31	~10
100	0.14±0.03	0.15	-14	~100	0.10±0.01	0.11	53	~10
150	0.15±0.02	0.16	-32	~100	0.12±0.02	0.14	56	~10
200	0.13±0.01	0.14	-28	~100	0.12±0.02	0.13	56	~10

Table 1. The summary of BGBC OTFT performance of **P4**. Average mobility obtained from five parallel devices at a V_{DS} of -100 V for p-channel operation and +100 V for n-channel operation.

View Article Online
DOI: 10.1039/C7TC03584E

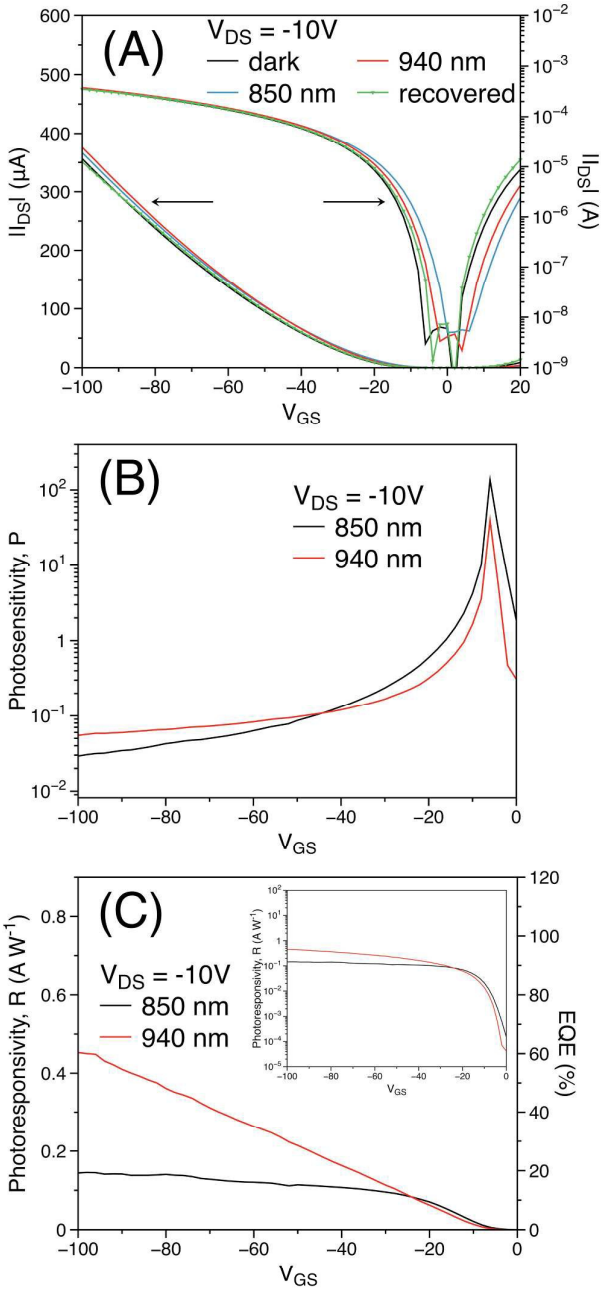

Figure 5. (A) The transfer curves of **P4** OPT illuminated with 850 nm and 940 nm light sources. The photosensitivity (P) (B), photoresponsivity (R), and external quantum efficiency (EQE) (C) as a function of V_{GS} measured for **P4**. Inset: the logarithmic form of R.

with Au source and drain patterns. The electrical characteristics were measured for devices after annealing at different temperatures for 20 min in nitrogen. OTFT figures of merit (μ, V_{th}, and I_{on}/I_{off}), measured in the saturation regime on the reverse scans of the transfer curves at V_{DS} = –100 V, are listed in Table 1. **P4** showed ambipolar charge transport characteristics with quite balanced hole and electron mobilities. All devices showed quite repeatable charge carrier mobilities with relative standard deviations of ~10-20%. The polymer film annealed at 50 °C showed hole and electron mobilities of up to 0.15 cm^2 V^{-1} s^{-1} and 0.12 cm^2 V^{-1} s^{-1}, respectively. When the annealing temperature increased from 50 °C to 150 °C, the charge carrier mobility improved only slightly. The best performance was observed for a device at an annealing temperature of 150 °C, which showed the highest hole and electron mobility of 0.16 cm^2 V^{-1} s^{-1} and 0.14 cm^2 V^{-1} s^{-1}, respectively (Figure 4). At a higher annealing temperature of 200 °C, both hole and electron mobilities decreased slightly to 0.14 cm^2 V^{-1} s^{-1} and 0.13 cm^2 V^{-1} s^{-1}, respectively, which might be due to the worsened adhesion of the polymer to the substrate at a high annealing temperature. The dependence of mobility on V_{GS} for 150 °C-annealed devices is shown in Figure S8. The mobilities in the ambipolar regimes appear to be quite similar compared to the values in their respective unipolar operation regimes.

We performed a study of **P4** as an active channel layer in OPTs. The OPT performance measurements were carried out in the dark and under illumination using 850 nm and 940 nm centered light emitting diodes (LEDs), which have power densities of 15.2 mW cm^{-2} and 9.1 mW cm^{-2}, respectively. Figure 5(A) shows the linear regime transfer curve of an OPT based on **P4** under p-channel operation, both in linear and logarithmic form, in response to the illumination of the two light sources, respectively. With both light sources, the drain current (I_{DS}) of the OPTs increases due to the generation of photo-generated carriers. A shift in the threshold voltage (V_{TH}) is observed, which is due to the photovoltaic effect.[49,50]

The large changes in I_{DS} strongly supports that **P4** is an excellent active channel layer for NIR detection. Based on the transfer curves measured in the dark and under illumination several OPT parameters, photosensitivity (*P*), photoresponsivity (*R*), and external quantum efficiency (*EQE*), can be quantitatively extracted using the following equations:[51,52]

$$P = \frac{I_{light} - I_{dark}}{I_{dark}} \quad (1)$$

$$R = \frac{I_{light} - I_{dark}}{P_{inc} W L} \quad (2)$$

$$EQE = R\left(\frac{hc}{\lambda_{peak} e}\right) \quad (3)$$

where I_{light} and I_{dark} are the I_{DS} under illumination and in the dark, respectively, P_{inc} is the incident illumination power density on the channel of the device, *W* and *L* are the channel width (15800 μm) and length (30 μm), *h* is Planck's constant (6.62607 × 10^{-34} m^2 kg s^{-1}), *c* is the speed of light in vacuum, *e* is the elementary charge (1.60218 × 10^{-19} C), and λ_{peak} is the wavelength of incident light with maximum intensity. For the convenience of the *EQE* calculation, the light sources were assumed to be monochromatic with a λ_{peak} of 850 nm and 940 nm, similar to the method ascribed by Labram *et al.*[51]

View Article Online
DOI: 10.1039/C7TC03584E

Polymer	Light source	Photosensitivity (P)	Photoresponsivity (R)	Ref.
P4 (this work)	850 nm	~100	145 mA W^{-1}	
	940 nm	~50	450 mA W^{-1}	
PBIBDF-TT	808 nm	10	20 mA W^{-1}	44
PBIBDF-TT (nanowire)	808 nm	2.3×10^4	440 mA W^{-1}	
PPQ2T-BT-24	579 nm	~100	800 mA W^{-1}	70
DPP-DTT (nanowire)	850 nm	1180	246 A W^{-1}	15
PPhTQ	White	0.5	400 A W^{-1}	33
DPPBTSPE	632 nm	~10^5	~2 A W^{-1}	54
DPPBTSPE (nanowire)	632 nm	~10^3	1920 A W^{-1}	

Table 2. The photoresponse of polymer based OPTs.

Figure 5(B) and (C) show the *P*, *R*, and *EQE* values as functions of the gate voltage (V_{GS}). A maximum *P* of about 10^2 is measured for both light sources. The slightly larger *P* measured with the 850 nm light source may be attributed to the greater power density, 15.2 mW cm^{-2}, oppose to 9.1 mW cm^{-2} for the 940 nm light source. **P4** also shows high NIR-IR sensitivity with *R*'s of 145 mA W^{-1} (120 mA W^{-1} on average) and 450 mA W^{-1} (387 mA W^{-1} on average) for 850 nm and 940 nm, respectively, with corresponding EQE's of 20% and 60%. *R* can be tuned from 10^{-4} A W^{-1} to about 1 A W^{-1}, over five orders, by modulating the V_{GS} (Figure 5(C)). Large gate-tunability is ideal for practical applications as it allows tunability of the photocurrent gain in respect to the incident light intensity.[17,53–55]

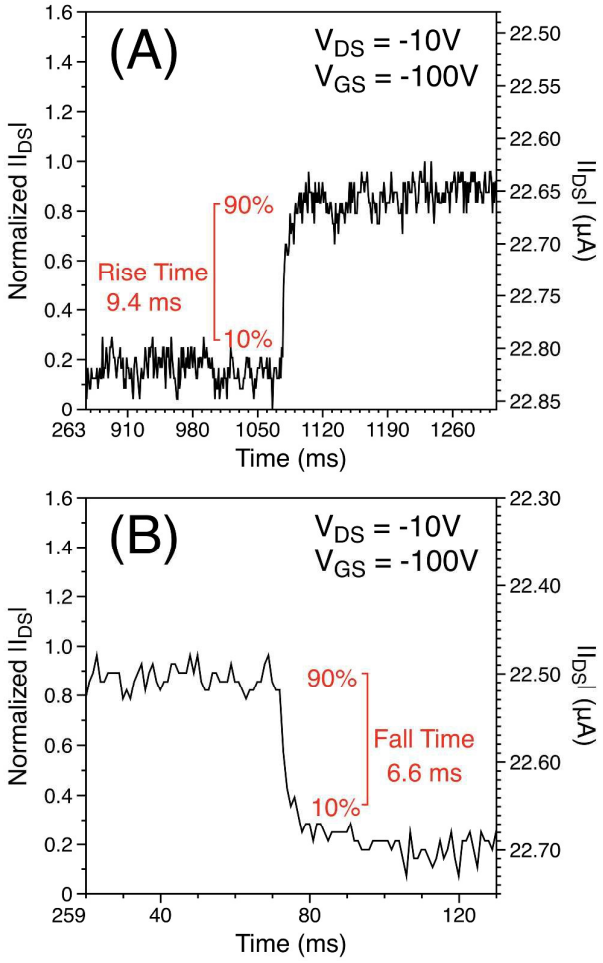

Figure 6. The rise (A) and fall time (B) of **P4** under 940 nm illumination at a V_{DS} = -10 V and V_{GS} = -100 V.

The transient photo-response of OPTs was also carried out to determine the response speed of the devices. The growth and decay components in the time response silhouettes, shown in Figure 6, reflect the photo-response promptness of the OPTs operated at V_{DS} = -10 V and V_{GS} = -100 V in response to the 940 nm light source. The rise time simply defined as the time taken from the I_{DS} at 10% to 90% of its maximum light on-state value while the opposite is defined for the fall time.[56] The shortest rise time extracted from the transient photo-response measurements was 9.4 ms with a corresponding fall time of 6.6 ms. These response times are among the best values reported in literature[57,58] and demonstrate that **P4** is a promising active channel layer for NIR OPTs to be used in the medical diagnosis, drug delivery and therapy.[59–62]

We also tested the OPT devices in the n-channel operation mode. However, a decrease, instead of increase, in I_{DS} was observed under illumination with either the 850 nm or 940 nm LED light source (Figure S9). Negative photoresponses have more frequently been reported for PTs based on inorganic semiconductors, which have been considered due to the charge carrier trapping.[63–67] Likewise, Tsai *et al.* observed negative photoresponses on pentacene based OPTs, where the OPTs showed an enhancement of I_{DS} in the p-channel operation and a suppression of I_{DS} in the n-channel operation in comparison to the devices measured in dark.[68] The cause of the decreased I_D was explained by the increased number of trapped electrons in the grain boundaries of the semiconductor layer and at the semiconductor/dielectric

View Article Online
DOI: 10.1039/C7TC03584E

interface induced by the illumination, which electrostatically shield the effective electrical field applied between the gate and source electrodes. [68] The higher sensitivity of electrons to the trap sites with respective to holes for pentacene was attributed to the observation. Therefore, the negative photoresponses observed for the **P4**-based OPTs may also be explained by the charge trapping. Our polymer **P4** has a LUMO energy of -3.86 eV, which is slightly lower than the minimum value of ca. -4.0 eV[48] required for a stable n-type organic semiconductor and thus is still sensitive to electron traps, which led the similar suppression of electron transport under illumination.

Experimental

Materials and characterization

All chemicals were obtained from commercial sources and used as received. (3,3'-bis(dodecyloxy)-[2,2'-bithiophene]-5,5'-diyl)bis(trimethylstannane)[47] and 3,7-bis((*E*)-6-bromo-1-(2-decyltetradecyl)-2-oxoindolin-3-ylidene)-3,7-dihydrobenzo[1,2-*b*:4,5-*b*']difuran-2,6-dione[34] were prepared according to the literature methods. High-temperature gel permeation chromatography (HT-GPC) measurements were performed on a Malvern 350 HT-GPC system using 1,2,4-trichlorobenzene as eluent and polystyrene as standards at a column temperature of 140 °C. Thermogravimetric analysis (TGA) was carried out on a TA Instruments SDT 2960 at a scan rate of 10 °C min^{-1} under nitrogen. Differential scanning calorimetry (DSC) was carried out on a TA Instruments Q2000 at a temperature ramping rate of 20 °C min^{-1} under nitrogen. The UV-Vis absorption spectra of the polymer were recorded on a Thermo Scientific model GENESYS™ 10S VIS spectrophotometer. Cyclic voltammetry (CV) data was collected on a CHI600E electrochemical analyser using an Ag/AgCl reference electrode and two Pt disk electrodes as the working and counter electrodes in a 0.1 M tetrabutylammonium hexafluorophosphate solution in acetonitrile at a scan rate of 50 mV s^{-1}. Ferrocene was used as the reference, which has a HOMO energy value of -4.8 eV.[69] The nuclear magnetic resonance (NMR) spectrum was obtained with a Bruker DPX 300 MHz spectrometer with chemical shifts relative to tetramethylsilane (TMS, 0 ppm). Reflective X-ray diffraction (XRD) measurements were carried out on a Bruker D8 Advance diffractometer with Cu Kα radiation (λ = 0.15406 nm) using polymer films spin coated on SiO_2/Si substrates. Atomic force microscopy (AFM) images were taken with a Dimension 3100 scanning probe microscope. To measure the photo response of the devices, the commercially available 5W 850 nm and 940 nm LEDs were used as the light source. A radiometer (model PMA2200) and pyranometer (model PMA2141) combination unit from Solar Light was used to determine the power density of the LED light sources. All theoretical calculations were carried out by using the Gaussian 09 suite of programs. The molecular geometries of the dimers and related calculations were performed by density functional theory (DFT) method using B3LYP functional group and 6-31G(d) as the basis set.

OTFT device fabrication and characterization

The bottom-contact bottom-gate (BGBC) configuration was used for all OTFT devices. The preparation procedure of the substrate and device is as follows. A heavily n^{++}-doped Si wafer with an ~300 nm-thick SiO_2 layer was patterned with gold source and drain pairs by conventional photolithography and thermal deposition. Then the substrate was treated with air plasma, followed by cleaning with acetone and isopropanol in an ultrasonic bath. Subsequently, the substrate was placed in a 3% dodecyltrichlorosilane (DDTS) solution in toluene at room temperature for 20 min. The substrate was washed with toluene and dried under a nitrogen flow. Then a polymer solution in chloroform (5 mg mL^{-1}) was spin-coated onto the substrate at 3000 rpm for 80 s to give a polymer film (~40 nm), which was further subjected to thermal annealing at different temperatures for 20 min in a glove box. All OTFT devices were characterized in the same glove box using an Agilent B2912A semiconductor analyser. The hole and electron mobilities are calculated in the saturation regime according to the following equation:

$$I_{DS} = \frac{\mu C_i W}{2L}(V_{GS} - V_{TH})^2$$

where I_{DS} is the drain–source current, μ is the charge carrier field-effect mobility, C_i is the gate dielectric layer capacitance per unit area (~11.6 nF cm^{-2}), V_{GS} is the gate voltage, V_{TH} is the threshold voltage, L is the channel length (30 μm), and W is the channel width (15.8 mm). The OPT (under illumination) devices were characterized in the same glove box where they were fabricated.

Synthetic procedure for PIBDFBTO-HH (P4)

To a 25 mL 2-necked Schlenk flask, 3,7-bis((*E*)-6-bromo-1-(2-decyltetradecyl)-2-oxoindolin-3-ylidene)-3,7-dihydrobenzo[1,2-*b*:4,5-*b*']difuran-2,6-dione (64.0 mg, 0.050 mmol), (3,3'-bis(dodecyloxy)-[2,2'-bithiophene]-5,5'-diyl)bis(trimethylstannane) (0.043 g, 0.050 mmol) and P(*o*-tolyl)$_3$ (1.3 mg, 4.0 μmol) were charged. After degassing and refilling with argon, $Pd_2(dba)_3$ (0.9 mg, 1.0 μmol) and anhydrous chlorobenzene (4 mL) were added and the mixture was stirred for 48 h at 130 °C. Upon cooling to room temperature, the reaction mixture was poured into methanol and the precipitate was collected by filtration. The crude polymer was purified by Soxhlet extraction using acetone, hexanes and chloroform successively. The chloroform fraction was dried in vacuum affording **P4** as a dark solid. Yield: 80 mg, 98%.

Conclusions

A small band gap D-A polymer, **PIBDFBTO-HH** (**P4**), was successfully synthesized using IBDF and a strategically chosen head-to-head alkoxy substituted bithiophene (BTO) as the co-

View Article Online
DOI: 10.1039/C7TC03584E

building blocks. The UV-Vis-NIR absorption spectra of **PIBDFBTO-HH** showed broad absorption in the NIR region up to ~1700 nm. As a channel material in OTFTs, it showed ambipolar performance. The highest hole mobility of 0.16 $cm^2 V^{-1} s^{-1}$ and the highest electron mobility of 0.14 $cm^2 V^{-1} s^{-1}$ were achieved. When used as an active material in OPTs, **PIBDFBTO-HH** exhibited a photosensitivity (P) as high as 130 and 40 under the illumination of 850 nm and 940 nm LED, respectively. A photoresponsivity of 450 mA W^{-1} together with response times of 9.4 ms for the rise time and 6.6 ms for the fall time were achieved under the 940 nm LED. Our results demonstrate that **PIBDFBTO-HH** is a promising material for NIR detection application.

Acknowledgements

This work is supported by the Natural Sciences and Engineering Research Council (NSERC) of Canada (Discovery Grants # RGPIN-2016-04366).

Notes and references

1 Y. Li, P. Sonar, L. Murphy and W. Hong, *Energy Environ. Sci.*, 2013, **6**, 1684–1710.
2 C. Guo, W. Hong, H. Aziz and Y. Li, *Rev. Adv. Sci. Eng.*, 2012, **1**, 200–224.
3 C. Wang, H. Dong, W. Hu, Y. Liu and D. Zhu, *Chem. Rev.*, 2012, **112**, 2208–2267.
4 A. J. Heeger, *Chem. Soc. Rev.*, 2010, **39**, 2354–2371.
5 A. C. Arias, J. D. MacKenzie, I. McCulloch, J. Rivnay and A. Salleo, *Chem. Rev.*, 2010, **110**, 3–24.
6 B. Sun, W. Hong, Z. Yan, H. Aziz and Y. Li, *Adv. Mater.*, 2014, **26**, 2636–2642.
7 Y. Gao, X. Zhang, H. Tian, J. Zhang, D. Yan, Y. Geng and F. Wang, *Adv. Mater.*, 2015, **27**, 6753–6759.
8 G. Kim, S.-J. Kang, G. K. Dutta, Y.-K. Han, T. J. Shin, Y.-Y. Noh and C. Yang, *J. Am. Chem. Soc.*, 2014, **136**, 9477–9483.
9 T. Lei, J.-H. Dou, X.-Y. Cao, J.-Y. Wang and J. Pei, *Adv. Mater.*, 2013, **25**, 6589–6593.
10 Y. He, W. Hong and Y. Li, *J. Mater. Chem. C*, 2014, **2**, 8651–8661.
11 X. Guo, M. Baumgarten and K. Müllen, *Prog. Polym. Sci.*, 2013, **38**, 1832–1908.
12 F. Yu, S. Wu, X. Wang, G. Zhang, H. Lu and L. Qiu, *RSC Adv.*, 2017, **7**, 11572–11577.
13 H. Hwang, H. Kim, S. Nam, D. D. C. Bradley, C.-S. Ha and Y. Kim, *Nanoscale*, 2011, **3**, 2275–2279.
14 T. D. Anthopoulos, *Appl. Phys. Lett.*, 2007, **91**, 113513.
15 Y. Lei, N. Li, W.-K. E. Chan, B. S. Ong and F. Zhu, *Org. Electron.*, 2017, **48**, 12–18.
16 B. Mukherjee, *Opt. - Int. J. Light Electron Opt.*, 2017, **139**, 48–55.
17 H. Xu, J. Li, B. H. K. Leung, C. C. Y. Poon, B. S. Ong, Y. Zhang and N. Zhao, *Nanoscale*, 2013, **5**, 11850–5.
18 T. Pal, M. Arif and S. I. Khondaker, *Nanotechnology*, 2010, **21**, 325201.
19 S. M. Mok, F. Yan and H. L. W. Chan, *Appl. Phys. Lett.*, 2008, **93**, 1–4.
20 E. C. P. Smits, S. Setayesh, T. D. Anthopoulos, M. Buechel, W. Nijssen, R. Coehoorn, P. W. M. Blom, B. de Boer and D. M. de Leeuw, *Adv. Mater.*, 2007, **19**, 734–738.
21 K. H. Hendriks, W. Li, M. M. Wienk and R. A. J. Janssen, *J. Am. Chem. Soc.*, 2014, **136**, 12130–12136.
22 P. H. Wobkenberg, J. G. Labram, J.-M. Swiecicki, K. Parkhomenko, D. Sredojevic, J.-P. Gisselbrecht, D. M. de Leeuw, D. D. C. Bradley, J.-P. Djukic and T. D. Anthopoulos, *J. Mater. Chem.*, 2010, **20**, 3673–3680.
23 Z. Sun, J. Li and F. Yan, *J. Mater. Chem.*, 2012, **22**, 21673–21678.
24 A. Rogalski, *Acta Phys. Pol. A*, 2009, **116**, 389–406.
25 Y. Peng, W. Lv, B. Yao, G. Fan, D. Chen, P. Gao, M. Zhou and Y. Wang, *Org. Electron.*, 2013, **14**, 1045–1051.
26 B. Sun, W. Hong, C. Guo, S. Sutty, H. Aziz and Y. Li, *Org. Electron.*, 2016, **37**, 190–196.
27 H. Yan, B. A. Collins, E. Gann, C. Wang, H. Ade and C. R. McNeill, *ACS Nano*, 2012, **6**, 677–688.
28 F. Li, Y. Chen, C. Ma, U. Buttner, K. Leo and T. Wu, *Adv. Electron. Mater.*, 2016, 1600430.
29 E. Bundgaard and F. C. Krebs, *Sol. Energy Mater. Sol. Cells*, 2007, **91**, 954–985.
30 H. A. M. van Mullekom, J. A. J. M. Vekemans, E. E. Havinga and E. W. Meijer, *Mater. Sci. Eng. R Reports*, 2001, **32**, 1–40.
31 L. Biniek, B. C. Schroeder, C. B. Nielsen and I. McCulloch, *J. Mater. Chem.*, 2012, **22**, 14803–14813.
32 H. A. M. van Mullekom, J. A. J. M. Vekemans and E. W. Meijer, *Chem. – A Eur. J.*, 1998, **4**, 1235–1243.
33 M. Li, C. An, T. Marszalek, X. Guo, Y.-Z. Long, H. Yin, C. Gu, M. Baumgarten, W. Pisula and K. Müllen, *Chem. Mater.*, 2015, **27**, 2218–2223.
34 Z. Yan, B. Sun and Y. Li, *Chem. Commun.*, 2013, **49**, 3790–3792.
35 T. Lei, J.-H. Dou, X.-Y. Cao, J.-Y. Wang and J. Pei, *J. Am. Chem. Soc.*, 2013, **135**, 12168–12171.
36 J.-H. Dou, Y.-Q. Zheng, T. Lei, S.-D. Zhang, Z. Wang, W.-B. Zhang, J.-Y. Wang and J. Pei, *Adv. Funct. Mater.*, 2014, **24**, 6270–6278.
37 G. Zhang, P. Li, L. Tang, J. Ma, X. Wang, H. Lu, B. Kang, K. Cho and L. Qiu, *Chem. Commun.*, 2014, **50**, 3180–3183.
38 T. Lei, X. Xia, J.-Y. Wang, C.-J. Liu and J. Pei, *J. Am. Chem. Soc.*, 2014, **136**, 2135–2141.
39 Y. He, C. Guo, B. Sun, J. Quinn and Y. Li, *Polym. Chem.*, 2015, **6**, 6689–6697.
40 G. Zhang, J. Guo, M. Zhu, P. Li, H. Lu, K. Cho and L. Qiu, *Polym. Chem.*, 2015, **6**, 2531–2540.
41 X. Zhou, N. Ai, Z.-H. Guo, F.-D. Zhuang, Y.-S. Jiang, J.-Y. Wang and J. Pei, *Chem. Mater.*, 2015, **27**, 1815–1820.
42 Y.-Q. Zheng, T. Lei, J.-H. Dou, X. Xia, J.-Y. Wang, C.-J. Liu and J. Pei, *Adv. Mater.*, 2016, **28**, 7213–7219.
43 X. Wang, H. H. Choi, G. Zhang, Y. Ding, H. Lu, K. Cho and L. Qiu, *J. Mater. Chem. C*, 2016, **4**, 6391–6400.
44 M. Zhu, S. Lv, Q. Wang, G. Zhang, H. Lu and L. Qiu, *Nanoscale*, 2016, **8**, 7738–7748.

View Article Online
DOI: 10.1039/C7TC03584E

45 D. H. Sliney, R. T. Wangemann, J. K. Franks and M. L. Wolbarsht, *J. Opt. Soc. Am.*, 1976, **66**, 339–341.
46 M. J. Frisch, *Gaussian 09 Revision A.02*, Gaussian, Inc., Wallingford CT, 2016.
47 X. Guo, J. Quinn, Z. Chen, H. Usta, Y. Zheng, Y. Xia, J. W. Hennek, R. P. Ortiz, T. J. Marks and A. Facchetti, *J. Am. Chem. Soc.*, 2013, **135**, 1986–1996.
48 B. A. Jones, A. Facchetti, M. R. Wasielewski and T. J. Marks, *J. Am. Chem. Soc.*, 2007, **129**, 15259–15278.
49 H.-S. Kang, C.-S. Choi, W.-Y. Choi, D.-H. Kim and K.-S. Seo, *Appl. Phys. Lett.*, 2004, **84**, 3780–3782.
50 Y. Takanashi, K. Takahata and Y. Muramoto, *IEEE Trans. Electron Devices*, 1999, 46, 2271–2277.
51 J. G. Labram, P. H. Wöbkenberg, D. D. C. Bradley and T. D. Anthopoulos, *Org. Electron.*, 2010, **11**, 1250–1254.
52 Y. Guo, C. Du, G. Yu, C. Di, S. Jiang, H. Xi, J. Zheng, S. Yan, C. Yu, W. Hu and Y. Liu, *Adv. Funct. Mater.*, 2010, **20**, 1019–1024.
53 H. Xu, J. Wu, Q. Feng, N. Mao, C. Wang and J. Zhang, *Small*, 2014, **10**, 2300–2306.
54 W. D. and W. D. O. and J.-C. B. and I. C. and W. M. and H.-G. B. and J. D. and M. N. and J. Manca, *Nanotechnology*, 2015, **26**, 65201.
55 X. Li, J. Wu, N. Mao, J. Zhang, Z. Lei, Z. Liu and H. Xu, *Carbon N. Y.*, 2015, **92**, 126–132.
56 Z. Qi, J. Cao, H. Li, L. Ding and J. Wang, *Adv. Funct. Mater.*, 2015, **25**, 3138–3146.
57 Z. Sun, Z. Liu, J. Li, G. Tai, S.-P. Lau and F. Yan, *Adv. Mater.*, 2012, **24**, 5878–5883.
58 G. Konstantatos, M. Badioli, L. Gaudreau, J. Osmond, M. Bernechea, F. P. G. de Arquer, F. Gatti and F. H. L. Koppens, *Nat Nano*, 2012, **7**, 363–368.
59 L. Cheng, K. Yang, Q. Chen and Z. Liu, *ACS Nano*, 2012, **6**, 5605–5613.
60 J. Zhou, Z. Lu, X. Zhu, X. Wang, Y. Liao, Z. Ma and F. Li, *Biomaterials*, 2013, **34**, 9584–9592.
61 T. Lee, D. Bang, Y. Park, S. H. Kim, J. Choi, J. Park, D. Kim, E. Kim, J.-S. Suh, Y.-M. Huh and S. Haam, *Adv. Healthc. Mater.*, 2014, **3**, 1408–1414.
62 H. Gong, L. Cheng, J. Xiang, H. Xu, L. Feng, X. Shi and Z. Liu, *Adv. Funct. Mater.*, 2013, **23**, 6059–6067.
63 B. Li, X. Yan, X. Zhang, Y. Luo, Q. Lu and X. Ren, *Appl. Phys. Lett.*, 2017, **111**, 113102.
64 P.-H. Chang, S.-Y. Liu, Y.-B. Lan, Y.-C. Tsai, X.-Q. You, C.-S. Li, K.-Y. Huang, A.-S. Chou, T.-C. Cheng, J.-K. Wang and C.-I. Wu, *Sci. Rep.*, 2017, **7**, 46281.
65 N. Guo, W. Hu, L. Liao, S. Yip, J. C. Ho, J. Miao, Z. Zhang, J. Zou, T. Jiang, S. Wu, X. Chen and W. Lu, *Adv. Mater.*, 2014, **26**, 8203–8209.
66 L. Tao, Z. Chen, X. Li, K. Yan and J.-B. Xu, *npj 2D Mater. Appl.*, 2017, **1**, 19.
67 C. Biswas, H. Jeong, M. S. Jeong, W. J. Yu, D. Pribat and Y. H. Lee, *Adv. Funct. Mater.*, 2013, **23**, 3653–3660.
68 T.-D. Tsai, C.-Y. Huang, H.-M. Lin, T.-F. Guo and T.-C. Wen, *Org. Electron.*, 2014, **15**, 3805–3810.
69 J. Pommerehne, H. Vestweber, W. Guss, R. F. Mahrt, H. Bassler, M. Porsch and J. Daub, *Adv. Mater.*, 1995, **7**, 551–554.
70 J. T. E. Quinn, F. Haider, H. Patel, D. A. Khan, Z. Y. Wang and Y. Li, *J. Mater. Chem. C*, 2017, **5**, 8742–8748.

View Article Online
DOI: 10.1039/C7TC03584E

Graphical abstract

A novel small bandgap donor-acceptor polymer with a very small band gap of 0.95 eV shows promising photoresponse under a near infrared light in phototransistors.